Genome Biology

https://doi.org/10.1186/s13059-026-03957-8

Article in Press

Genetic dynamics drive maize growth and breeding

Received: 06 Jul 2025

Accepted: 13 Jan 2026

Published online: 29 January 2026

Cite this article as: Wu, C., Geng, Z., Li, W. *et al.* Genetic dynamics drive maize growth and breeding. *Genome Biol* (2026). https://doi.org/10.1186/s13059-026-03957-8

Chengxiu Wu, Zedong Geng, Weikun Li, Junli Ye, Xiaoyuan Hao, Jieting Xu, Minliang Jin, Xiaoyu Wu, Yuanhao Du, Yunyu Chen, Cheng Ma, Yu Gao, Yuyue Chen, Tianjin Xie, Songtao Gui, Yuanyuan Chen, Jingyun Luo, Yupeng Liu, Wenyu Yang, Jianbing Yan, Wanneng Yang & Yingjie Xiao

Genetic dynamics drive maize growth and breeding

Chengxiu Wu (吴成秀)[1,2†], Zedong Geng (耿泽栋)[1,2†], Weikun Li (李为坤)[1,2], Junli Ye (叶军立)[1,2], Xiaoyuan Hao (郝小媛)[1], Jieting Xu (许洁婷)[6], Minliang Jin (金敏亮)[6], Xiaoyu Wu (吴晓昱)[6], Yuanhao Du (杜沅昊)[1], Yunyu Chen (陈韵宇)[1], Cheng Ma (马骋)[1], Yu Gao (高豫)[1], Yuyue Chen (陈昱月)[1], Tianjin Xie (谢田晋)[1], Songtao Gui (桂松涛)[4], Yuanyuan Chen (陈园园)[5], Jingyun Luo (罗靓赟)[3], Yupeng Liu (刘玉鹏)[1], Wenyu Yang (杨文宇)[1], Jianbing Yan (严建兵)[1,2*], Wanneng Yang (杨万能)[1,2*], Yingjie Xiao (肖英杰)[1,2*]

*Correspondence should be addressed to Jianbing Yan (yjianbing@mail.hzau.edu.cn); Wanneng Yang (ywn@mail.hzau.edu.cn); Yingjie Xiao (yxiao25@mail.hzau.edu.cn)

[†]These authors contributed equally to this work

[1]National Key Laboratory of Crop Genetic Improvement, Huazhong Agricultural University, Wuhan, 430070, China

Full list of author information is available at the end of the article

Abstract

Background: Phenotypic diversity arises from the process of development and is shaped by genomic variation in plants. However, the genetic basis of growth dynamics remains poorly understood in maize.

Results: Here, we analyze 679 maize inbred lines derived from a synthetic CUBIC population with approximately 2.8 million SNPs, leveraging high-throughput

phenotyping to capture 1,002,240 RGB images across 18 growth stages. We quantify 67 image-based traits (i-traits), revealing distinct dynamic patterns throughout development. Genome-wide association studies identify 857 quantitative trait loci (QTLs) influencing growth variation, with 88.6% classified as period-specific dynamic QTLs exhibiting modest effects, and 11.4% as conservative QTLs with sustained effects. Notably, 1.5% of cryptic pleiotropic QTLs spanning different growth stages suggest genetic relocations during development. These QTLs enhance heritability estimates for mature traits by an average of 6.2%. We further characterize the novel function of key genes linked with these QTLs, including *BRD1* with the pleiotropic effects on plant height and perimeter of convex hull and *ZmGalOx1* with the broad-spectrum regulation of plant architecture. Developmental rewiring of epistatic networks shapes maize growth, underscoring the vitality of temporal genetic regulation. Trajectory modeling of i-traits across periods decodes the growth variation patterns, supporting the ontogenic hypothesis driven predictive breeding strategies.

Conclusion: The findings elucidate the genetic architecture underlying growth dynamics from a spatial-temporal perspective, offering novel insights for maize improvement.

Key words: Maize, Image-based traits, Growth dynamics, Temporal genetic regulation, Trajectory modeling, Breeding design

Background

Maize (*Zea mays*) is a globally vital crop, serving as a critical source of food, feed, and industrial raw materials. With rising global demand for maize, continuous improvement of agriculturally important traits is essential to meet the needs of a growing population [1, 2]. Deciphering the genetic basis of these agronomic traits and cloning their underlying genes remains an important measure to address these needs [3]. Over the past decades, the maize research community had made significant contributions in functional genomics, identifying hundreds of genes and natural variants responsible for agronomic traits [4]. Most agronomic traits are quantitatively inherited, conforming to the polygenic hypothesis, wherein phenotypic variation arises from the cumulative effects of numerous minor loci and their interactions [5]. For instance, the maize grain yield is estimated to be influenced by thousands of minor-effect genes [6], suggesting that a substantial proportion of heritability remains unexplained. The omnigenic hypothesis, originally proposed in human genetics, offers a framework for interpreting complex traits. According to this hypothesis, trait variation is governed by two interconnected gene networks: (1) core genes with direct biological relevance to the trait, and (2) peripheral genes that influence the trait indirectly through interactions with core genes or by modulating related biological processes [7]. This paradigm may also prove valuable for dissecting complex agronomic traits in plants. Traditionally, studies had predominantly focused on the endpoint traits measured at harvest, surely indirectly shaped by underlying growth

attributes. However, the genetic architecture and functional importance of these dynamic growth-related traits remain poorly understood.

Advances in high-throughput phenotyping (HTP) platform have enabled large-scale and dynamic characterization of plant growth attributes, providing unprecedented opportunities to decode the genetic basis of agronomic traits [8]. Time-resolved genetic studies in *Arabidopsis*, barley, *Brassica napus*, cotton, and wheat have revealed that many quantitative trait loci (QTLs) exhibit the temporal specificity with shifted effects across developmental stages [9-15]. In maize, recent efforts have leveraged the UAV-based phenotyping and mathematical modeling to identify genomic regions associated with vegetative growth and flowering [16, 17]. A landmark study of 368 diverse inbred lines subjected to drought stress uncovered 1,529 QTLs linked to image-based traits, leading to functional validation of *ZmcPGM2* and *ZmFAB1A* as regulators of drought-tolerance in maize [18]. Overall, the above-mentioned studies have paid relatively more attention to the discovery of genes using the populations with less relevance to crop improvement.

In the present study, we employed the maize CUBIC (Complete-diallel plus Unbalanced Breeding-derived Inter-Cross) population that had been used as a powerful resource for genetic studies, heterosis exploration, and genomic breeding [19-21], to investigate growth dynamics across vegetative and reproductive phases. Using HTP platform, we identified 67 image-based traits (i-traits) over 18 continuous growth periods. Our study revealed diverse growth patterns among inbred lines and identified a comprehensive set of QTLs with distinct functional roles, which deepen

insights into the dynamic genetic architecture of quantitative traits and recover a substantial fraction of "missing heritability" overlooked by traditional trait–genome association approaches. The prevalent epistatic interactions play a pivotal role in shaping developmental status and identify *ZmEBF4* as a causal gene governing early-stage plant height. Based on the understanding of dynamic genetic nature for growth traits, we propose the ontogenic hypothesis by extending omnigenic hypothesis toward the temporal dimension, indicating the complex traits were determined by panoramic spatial-temporal interactions between key genes and epistatic pairs. Driven by ontogenic hypothesis and mathematical modeling, we provided a novel hybrid breeding strategy via asymmetric growth trajectory design in parents for future crop improvement.

Results

Diverse and dynamic i-traits capture the maize growth variation

To systematically characterize the maize growth diversity, we cultivated 679 randomly selected lines from the CUBIC population in an outdoor greenhouse (Additional file 1: Figure S1a). Using a plant-to-sensor HTP platform, we captured >1 million images across 18 growth stages from seedling stage (V4, 38 days after sowing) to mature stage (R4, 95 days after sowing), obtaining 67 i-traits through an integrated computational pipeline (Fig. 1a; see Methods) [18, 22-24]. This approach enabled

dynamic quantification of growth variation across different developmental stages, rather than relying solely on endpoint measurements at harvest.

The i-traits encompassed four categories – biomass, color, morphology and texture – providing comprehensive coverage of RGB-based plant features throughout development (Additional file 2: Table S1). Clustering analysis of 679 inbred lines revealed that agronomic trait profiles were distinct from patterns of genomic variation but similar with that of i-traits (Fig. 1b; Additional file 1: Figure S2), suggesting that i-traits may bridge genomic architecture and endpoint phenotypic causality following the central dogma in genetics.

Coefficient of variation (CV) analysis classified 67 i-traits into two groups based on bimodal distribution (Fig. 1c; Additional file 1: Figure S1b). The Group-I (lower variance than agronomic traits; p=9.6×10^{-3}) was enriched for texture related features, whereas the Group-II (higher variance than agronomic traits; p=1.3 × 10^{-4}) predominantly comprised morphological traits (Additional file 2: Table S2). For developmental staging, we partitioned the 18 time points into three stages, as early (V4-V10), middle (V10-R1), and late (R1-R4) (Additional file 1: Figure S1c; Additional file 2: Table S3).

Hierarchical clustering of normalized i-traits across periods revealed three distinct dynamic patterns: increasing, decreasing, and stable. (Fig. 1d). Traits of the increasing type (e.g., plant height and biomass) represented a cumulative growth pattern. In contrast, decreasing-type traits (e.g., perimeter/projected area ratio, PAR) primarily reflected morphological changes (Additional file 2: Table S4). These increasing traits

also showed significantly higher heritability, especially in late developmental stages—a pattern that may indicate distinct genetic regulation underlying different i-trait types (Additional file 2: Table S5). Principal component and correlation analyses further disclosed the phenotypic specificity among the three i-trait growth types (Additional file 1: Figure S1d-e), laying a foundation to dissect how dynamic features mediate genotype-to-phenotype relationships in maize.

Temporal dynamics of genetic architecture underlying i-traits

Variance component analysis revealed that developmental time accounted for the majority of global i-trait variations (55.4%), while exerted their strongest influence during late growth phases (Additional file 1: Figure S3). This suggests that early subtle genetic differences become magnified through subsequent growth, ultimately shaping the mature phenotypic diversity. Over 90% of i-traits showed substantial heritability (broad-sense heritability>0.5), with heritability significantly increasing in late developmental periods (Additional file 1: Figure S4; Additional file 2: Table S5), consistent with previous observations in maize [22].

Using 2,822,486 high-quality SNPs (MAF≥0.05), we performed genome-wide association study (GWAS) for all 67 i-traits across 18 time periods, identifying 857 QTLs ($p \leq 3.5 \times 10^{-7}$) (Fig. 2a). On average, two QTLs (range: 1 to 22) were identified for each i-trait, while 47 QTLs (range: 25-125) for each development stage were found (Additional file 2: Table S6). The number of detected QTLs peaked during middle developmental stage (125 QTLs at stage 7), significantly exceeding early- and

late-stage counts (p=8.4×10^{-4} and p=6.6×10^{-3}, respectively; Additional file 1: Figure S5a). Notably, the late-stage QTLs exhibited larger effect sizes than the early or middle-stage ones (Additional file 1: Figure S5b), including 10 major QTLs with phenotypic variance explained (PVE) over 10%. The QTL confident intervals spanned 0.05-44.03 Mb, 82.3% of which overlapped with genic regions (Additional file 1: Figure S5c). The identified QTLs across multiple stages were clustered into 24 genomic hotspots showing strong developmental specificity and enrichment for transcription factors (p<0.05; Additional file 1: Figure S5d-e).

For each i-trait, the original QTLs across development periods were merged into consensus QTL based on the colocalization analysis (r^2>0.2). Totally, 450 consensus intervals were obtained and further integrated into 263 unique genomic regions putatively regulating growth-related i-traits (see Methods, Additional file 2: Table S6). These QTLs exhibited two temporal patterns: (1) Dynamic QTLs (88.6%): Stage-specific associations (e.g., a chromosome 7 locus associated with Heywood circularity exclusively in late periods; Fig. 2c). (2) Conservative QTLs: Persistent effects across stages (e.g., a chromosome 4 region mapped by plant compactness throughout development; Fig. 2d).

Functionally, most QTLs were monotropic (associated with single i-trait), but 24.7% showed approximate pleiotropy—including four "cross-period pleiotropic" loci with stage-shifting effects (Fig. 2b; Additional file 2: Table S7). For example, a chromosome 1 QTL were associated with early-stage plant height but switched to be significantly associated with Heywood circularity after floral transition (Fig. 2e),

illustrating how developmental context reshapes the genetic contributions to the plant growth.

Conservative QTLs, though fewer in number, explained significantly more phenotypic variance than dynamic QTLs ($p<6.9\times10^{-6}$), while pleiotropic loci outperformed monotropic QTLs in explained variance per locus ($p<4\times10^{-3}$) (Fig. 2f). Combinations of conservative and pleiotropic QTLs dominated i-traits regulation (Additional file 1: Figure S5f), suggesting they may pinpoint the key structural genes or transcriptional hub factors. Including all stage-specific QTLs in regression models substantially improved variance explanation for mature traits—average variance increased from 7.9% to 14.1%, with maximal gains for plant compactness3 (PC3; 7.1%-29.2%)—better aligning with the estimated heritability (Additional file 2: Table S8).

Genetic architecture underlying distinct growth patterns of i-traits

We identified 130, 94 and 81 unique QTLs, associated with increasing, decreasing, and stable type of i-traits, respectively (Additional file 2: Table S6). The frequency of conservative QTLs was comparable between increasing and decreasing type of i-traits, but significantly lower for stable i-traits (Fig. 3a). This pattern was correlated with effect size differences, that conservative QTLs had larger effects on stable traits compared to other types, while dynamic QTL showed similar effect among i-trait types (Fig. 3a). The monotropic QTLs were enriched in stable i-traits rather than pleiotropic QTLs ($p<0.05$; Fig. 3b), suggesting that pleiotropic loci may preferentially

drive growth variability. The increasing and decreasing type of i-traits basically reflected the attributes during the plant growth, thus this result further indicated that the large number of modest variants with dynamic allelic spectrum reformed the plant status and accumulatively shaped the plant development.

We identified several key genes previously reported relevant to plant growth and development. *BRD1* was mapped to a conservative QTL on chromosome 1 with persistent effects on plant height (increasing-type trait) through middle and late stages. The PlantCompactness4 (PC4) as a decreasing i-trait detected *DLF1* with the function mediating floral inductive signals [25]. *GL15* – a known gene for leaf epidermal features (epicuticular waxes, leaf hairs) [26] – was mapped to a conservative QTL associated with the stable trait GPAR (Fig. 3c-e). The *ZmGalOx1* [19] for ear leaf width and *MADS69* (a flowering time regulator) [27] could play a role in a series of i-traits across all three growth types, highlighting the central role of pleiotropy in coordinating plant architecture and vegetative-to-productive transition.

Dynamic genetic regulation of maize plant architecture

Plant architecture is a critical determinant of crop productivity, with ideal plant architecture being increasingly targeted in modern breeding programs for high-density cultivation [28]. Leveraging our high-throughput phenotyping (HTP) platform, we investigated two key architectural features—leaf sparseness and plant height—throughout development to uncover their dynamic genetic regulation.

The architecture of lower leaf angle and upright leaf in the top is beneficial for grain yield production via improved photosynthesis in the population level [29]. *ZmGalOx1* located in the top of chromosome 4, encoded galactose oxidase that had been proved to control maize leaf width via regulating cell proliferation efficiency [19]. We found that *ZmGalOx1* was mapped to a significant locus responsible for both ear leaf width (ELW) and perimeter/projected area ratio (PAR) (Fig. 4a). PAR is an i-trait reflecting the sparseness of leaves in the plant. *ZmGalOx1* had kept the influential effect on leaf sparseness from early to late development periods (Fig. 4b). The expression profile of B73 indicated that *ZmGalOx1* is constitutively expressed in all tissues and development periods, with high expression mainly in the leaves and internodes during early growth periods (Additional file 1: Figure S6a). Interestingly, we found that *ZmGalOx1* were associated with multiple plant architecture-related i-traits, such as plant compactness (PC) and total projected area/bounding rectangle area (TBR) throughout entire growth periods (Fig. 4c; Additional file 2: Table S9). It indicated that *ZmGalOx1* underlies a locus for plant ideal architecture probably via coordinating systematic growth traits due to genetic pleiotropic regulations.

We edited *ZmGalOx1* using CRISPR–CasY7, an independently developed gene-editing system, in the inbred line Jing724, the female parent of commercial hybrid JingKe968 and obtained homozygous line carrying frame-shift mutation (*ZmGalOx1*-KO^{Jing724}). We had conducted full-growth-period phenotyping using the identical HTP for both the *ZmGalOx1*-KO^{Jing724} and wild-type Jing724. It was found that the knockout line of *ZmGalOx1* exhibited significant difference compared to the

wild type across plant architecture-related i-traits that had been identified association to the *ZmGalOx1* locus in our GWAS study—including PAR, plant compactness 1–6, TBR (Figure 4d-e; Additional file 1: Figure S7). This result genetically confirmed that *ZmGalOx1* not only influenced the ear leaf width as previously reported, but also functioned as the key gene regulating multiple i-traits across growth cycle, finally contributing to compact plant architecture suitable to dense planting.

Plant height is vital for dense planting breeding. GWAS detected *BRD1* (a plant height regulator*)* [30] significantly influencing plant height in the middle periods, which switched to be associated with the perimeter_convex.hull (The circumferential length of the convex hull enclosing the target object) in the late periods (Fig. 4f). To interpret the allelic spectrum along plant growth, we found the CC allele of *BRD1* (peak SNP: chr1.s_253169139) contributed to higher plant status than TT allele, while the additive effect of *BRD1* was incremental along development periods (Fig. 4g). It explained that traditional detectable effect of *BRD1* was probably due to accumulative effects initiated from early periods. Interestingly, we found that *BRD1* had switched its role from plant height to perimeter_convex.hull after floral transition (Fig. 4h), which provide putative explanation of active *BRD1* expression status in late periods (Additional file 1: Figure S6b). This result exemplifies the mechanism of functional relocation of *BRD1* to efficiently serve the genetic regulation of plant growth in maize.

Developmental rewiring of epistatic networks shapes maize growth

Epistatic interactions are an important yet underexplored source of complex traits in developmental genetics [19, 31, 32]. Our comprehensive analysis of pairwise QTL interactions (bi-QTL) uncovered 721 significant epistatic pairs (26.3% of tested interactions, $p<0.05/435$, 435 is the maximum number of tested bi-QTL for single trait) influencing i-traits across growth stages (Additional file 2: Table S10). These epistatic interactions exhibited striking temporal specificity, with most active in only 1-2 developmental stages (Additional file 2: Table S11), demonstrating greater stage-sensitivity than individual QTL effects. Notably, 10.2% of interacting pairs showed pleiotropic effects on multiple i-traits (Additional file 2: Table S12). The significant bi-QTLs could be further classified into three types (SS, SN, NN) based on the significance of each constituent QTL in testing time (Fig. 5a). Intriguingly, the majority of significant interactions (97.5%) involved loci that were non-significant in single-QTL analyses (Additional file 2: Table S10), suggesting extensive cryptic genetic variation masked by epistatic buffering. Incorporating these interactions into predictive models explained substantial additional ~10.2% heritability (maximum 35.3%; Additional file 2: Table S13).

The temporal development revealed progressive network complexity, with epistatic prevalence increasing from 15.4% in early stage to 40.5-49.9% in middle and late stages (Fig. 5b; Additional file 1: Figure S8). This expansion coincided with rising participation of large-effect loci (Additional file 2: Table S14), indicating that genetic networks are dynamically rewired to coordinate later-stage growth.

A striking example for interactive function was found in plant height. GWAS detected a major QTL (peak SNP: chr4.s_238092533; p=2.55×10^{-9}) at the end of chromosome 4 for early-phase plant height, which became undetectable in the late phase (Fig. 5c). Allelic effect analysis confirmed the early-stage specificity, with diminishing contributions after vegetative growth (Fig. 5d). Interestingly, alongside with it, a novel locus for plant height on chromosome 1 was found significant in the late phase but not early phase (Fig. 5c; Additional file 1: Figure S9a), implying epistatic interaction involved between them putatively. We indeed found two loci (chr4.s_238092533 and chr1.s_253261589) had interacted genetically with growing magnitude along the plant development (Additional file 2: Table S15). In the early phase, the interaction between them wasn't significant yet, the locus on chromosome 4 exhibiting strong effect on plant height (p=5×10^{-6}), probably due to the inactive status of the inhibitor (the locus on chromosome 1) (p=0.45); in the late phase, significant interaction emerged, when the locus on chromosome 1 carried the AA allele, the locus on chromosome 4 maintained its early-stage effect on plant height (PH). In contrast, if TT genotype for the chromosome 1 locus, the effect of the chromosome 4 locus on PH was reversed. Notably, it is statistical reliable to reveal the active haplotype had inhibited the detectable significance of the chromosome 4 locus on plant height (p=1.8×10^{-13}), as the sample size of inhibiting haplotype of the chromosome 1 locus was sufficiently large (n=361) (Fig. 5e; Additional file 1: Figure S9b-d). This inhibitor-relieve model probably explains the phenomenon of the

early-specific detectable locus on plant height, and previously reported relevant to heterosis formation in maize [20].

According to peak SNP position, gene expression and annotation, we proposed Zm00001d053642 to be the candidate gene responsible for the plant height QTL on chromosome 4 (Fig. 5f; Additional file 1: Figure S10-11). It encoded an EIN3-binding protein, *Arabidopsis* orthologs of Zm00001d053642 (*EBF1* and *EBF2*), influenced *Arabidopsis* early growth and plant height [33-35], thus termed as *ZmEBF4*. Interestingly, expression QTL analysis revealed that the *ZmEBF4* expression in V9 leaf was strongly impacted by cis-regulatory variants within the plant height QTL locus (Fig. 5f), further implying the causality of *ZmEBF4* on plant height. The mutant line (*ebf4*) carrying an EMS-induced premature stop codon (Additional file 1: Figure S12) was grown in Hainan and Xiangyang in 2023 and 2024. The homozygous mutant exhibited visibly shorter shorter height than the wild type in B73 background (Fig. 5g), and the phenotypic difference between mutant and wild type appeared to be larger in the early phase (V7-V8, p=1.4×10^{-4}) than late phase (R2-R3, p=0.014) (Fig. 5h) in Hainan, similar validating result was found in Xiangyang (Additional file 1: Figure S13). In summary, we identified a novel gene specifically functional in the early development, providing new gene resource for unraveling plant architecture and breeding.

The trajectory modeling integrating growth variation empower the breeding design

Traditional crop breeding has predominantly focused on maturity traits. Our findings, however, reveal that agronomic traits are underpinned by a complex developmental genetic architecture. Thus, we proposed the ontogenic hypothesis to explain and utilize agriculturally important traits, that complex traits are determined by panoramic spatial-temporal interactions between key genes and epistatic pairs. It's a challenge to depict the growth status along lifetime integrating the spatial-temporal dimensional i-trait data.

Through the increasing and decreasing type of i-traits based on Gompertz model, the growth trajectory for each inbred line was fitted by the parabolic function (median R^2=0.74, RMSE=0.0042), with three primeval function parameters (a, b, c) and two parabolic feature parameters ($-\frac{b}{2a}$ called 'axis of symmetry', $c-\frac{b^2}{4a}$ called extremum) (Fig. 6a-b). The five model parameters determined the growth pattern per line, termed as growth traits. The growth trait had significantly higher variation than original i-traits (p=0.03) (Additional file 2: Table S16), implying the majority of plant development information captured by the trajectory modeling. The growth traits exhibited significantly stronger correlation with i-traits in the middle and late phases than that in early phase (Fig. 6c and Additional file 1: Figure S14), probably reflecting the key contribution of floral transition phase to the diversity of growth trajectory.

Narrow-sense heritability (h^2) of growth trait was, on average, 0.026 higher than that of original i-traits (Additional file 1: Figure S15a), of which, the axis of

symmetry and parameter b had the highest heritability (h^2=0.411 and 0.407), implying the sufficient heritable ability of the growth trajectory. GWAS of growth traits detected 28 significant QTL loci at the stringent threshold ($p \leq 3.5 \times 10^{-7}$; Additional file 2: Table S17), encompassing several known genes relevant to plant growth and development (Fig 6d), but limited the jointly explained variance of 8.5-27.7% (Additional file 1: Figure S15b). At the suggestive threshold ($p \leq 3.9 \times 10^{-5}$), the growth traits detected a total of 235 suggestive QTL (Additional file 2: Table S18), greatly enhancing the explained variance to 62.8%-76.0% (Additional file 1: Figure S15c), significantly higher than by chance (Additional file 1: Figure S15d).

The ontogenic hypothesis guided us to better understand the genetics of complex traits, and further probably arise the new breeding design via spatial-temporal perspective rather than endpoint traits. The trajectory determined by three parameters provided the manageable potential of selection on the growth pattern in breeding use. To explore the potential of hybrid breeding, we predicted the values of three trajectory parameters for 207 maternal, 30 paternal lines and 6210 hybrids (Additional file 2: Table S19). We selected two distinct sets of 30 hybrids with top and bottom middle-parent heterosis (MPH) value based on ear weight from 6210 hybrid combinations [20]. The high-heterotic hybrids had significantly different trajectory parameters with the weak-heterotic hybrids (p=0.008 for a; p=0.065 for b) (Fig. 6e; Additional file 2: Table S20). The high-heterotic hybrids exhibited visible topologically difference between maternal and paternal trajectories, contrastingly similar between parents for weak-heterotic hybrids (Fig. 6f). However, the genetic

relatedness between maternal and paternal lines exhibited no significant difference between high-heterotic hybrid and weak-heterotic (0.0343 vs. 0.0197, p=0.51, Additional file 1: Figure S16). The result further implies the possible link between asymmetric parental trajectory and hybrid vigor, independent to traditional genotype complement. These results illuminated the potential of trajectory complement as new route for line improvement and hybrid breeding in maize.

Discussion

In this study, we achieved RGB image acquisition, trait extraction, and analysis of maize plants through high-throughput and automated experiments. However, the observed bidirectional clustering pattern indicates that, despite the large amount of data generated, the i-traits derived from time-series RGB images can ultimately capture only a limited set of information related to pixel intensity and size, resulting in a constrained feature correlation structure. There is still room for optimization in the technology. Although the equipment is initially automated, manual handling and management are still required. Additionally, the phenotypic algorithm uses traditional threshold segmentation, which has high limitations with regard to background environments. With the development of agricultural intelligence, the automation and intelligence of high-throughput phenotyping equipment have become the trend. To support the high-precise fundamental genetic research, the high-throughput phenotyping platform needs to keep increasing the efficiency and accuracy of data collection. The integrate automatic guided robot transport vehicles is better alternative

to boost the image screening throughput and further cut the labor costs. The art-of-state deep learning and image recognition approaches will benefit the accuracy on image segmentation and growth related i-trait extraction. Furthermore, for field crops such as maize, rice and wheat, the high-throughput field-scale phenotyping system was believed to be urgent technology for genetic study and breeding. The more field experiments combined with breeding practices and the application of modern phenomic detection techniques, such as Unmanned Aerial Vehicle and field sensors, aided by multi-modal AI analytic method, will have great potential for generating robust field-scale big data for future model improvement.

In recent years, with the rapid development of deep learning technology, more deep learning algorithms have played an important role in phenomics research. The continuous iteration and update of deep learning networks have provided sustained technical support for image segmentation and prediction, significantly improving accuracy and robustness. Therefore, in future research, datasets could be created for training deep learning networks such as SegFormer [36], U-Net [37], and Faster R-CNN [38]. These methods could process maize images not only to accurately segment the entire maize plant but also to precisely identify key organs such as the maize tassel and ear, facilitating comprehensive trait extraction and analysis.

Compared to natural populations, well-designed populations can significantly reduce the impact of population structure on GWAS and improve the detection power of causal variants [39]. Early artificial populations, such as nested association mapping (NAM) [40], random-open-parent association mapping (ROAM) [6], and the

multi-parent advanced generation intercross (MAGIC) populations [41, 42], have greatly enhanced the efficiency of causal variant detection and gene discovery in maize. More recently developed populations, including the CUBIC population [19] in maize and the 18K-rice population [32] in rice, have further minimized the influence of population structure while integrating diverse genetic variations, substantially advancing functional genomics research. In this study, we extended the utilization of maize CUBIC population to the genetic study of growth related phenomics, which comprehensively dissect the dynamic nature of plant growth variation with prevalent dynamic, pleiotropic QTLs and bi-QTL epistatic interactions.

The key question to answer in the plant breeding is the genetic architecture of the agricultural important trait. The hypotheses for complex traits formation directly determine interpreting trait variation and application in crop improvement.

Traditionally, the crop genetics and breeding follows the polygenic hypothesis, that realized the quantitative traits are governed by few major genes and numerous trivial genes [5]. It implied that trait improvement requires to consider the whole-genome variants rather than the few key loci, which guide the breeding paradigm reforming from marker-assisted selection (MAS) to genomic selection (GS). The functional genomics nowadays greatly help realizing the genetic effects of currently proved gene loci via multi-omics and molecular biology approaches [3, 43]. But it remains to be elusive on the global view why the set of genes across genomes appeared to be functionally distinct in allelic effect volume.

The omnigenic hypothesis provides a systematic explanation for polygenic model by extending single trait to multiple traits along spatial dimension [7]. The major gene had the substantial effect as it function directly on the target trait, while the genes with trivial effects perhaps indirectly influenced target trait by regulating the related traits. Thus, the functional major and trivial genes are interpreted to be spatially core and peripheral genes, respectively, based on the fact of their physical approximation to target trait. The hypothesis of omnigenic model reminds the vitality of systematic traits to the breeding, implying the reliability of transforming GS roadmap to the multiple-trait synergistic selection (MTSS) paradigm. The target-oriented prioritization (TOP) algorithm was an art-of-state MTSS approach for simultaneously selecting multiple traits in maize [21].

In the present study, we further extended the omnigenic hypothesis toward the temporal dimension, named as ontogenic hypothesis, which proposed that the complex traits were determined by panoramic spatial-temporal interactions between key genes and epistatic pairs (Additional file 1: Figure S17). We found the temporal related loci and genes were vital to systematically interpret the formation of complex traits at the endpoint and provided the alternative to partially address the long-term debate of “missing heritability”. Considerable QTLs and bi-QTL interaction served to be pleiotropy on the multiple i-traits, especially, engaging in cross-period pleiotropy, illuminating the mechanism of genetic relocations on plant growth regulation mediated by panoramic spatial-temporal interactions. Our findings provide new intriguing knowledge for the genetic architecture of the quantitative traits in maize.

The ontogenic hypothesis guided us to better understand the genetics of complex traits from spatial-temporal dimensions, and further probably arise the new breeding design via spatial-temporal perspective rather than endpoint traits. In traditional breeding practice, actually, breeders had indeed selected candidate lines for next cycle with similar logic, that not just by endpoint grain yield, but also multiple field traits expressed across different development periods. The high-throughput phenotyping technique allows us to efficiently collect image data comprehensively along the lifetime, but it's hard to make selection based on high dimensional features. Thus, we mathematically modeled the plant growth features into the trajectory determined by three parameters, this limited number of features provided the manageable potential of selection on the growth pattern in breeding use. Driven by ontogenic hypothesis, we empirically propose a novel route for hybrid breeding via asymmetric parental trajectory design in maize.

Conclusions

In this study, using a high-throughput phenotyping platform, a high-temporal-resolution RGB images investigation of 679 maize inbred lines were conducted throughout vegetative and reproductive phases. From these images, we extracted 67 image-based traits (i-traits) exhibiting diverse developmental patterns. By integrating genome-wide association studies, the dynamic genetic architecture was systematically dissected, and genetic effect relocation with growth was discovered. We further validated *ZmGalOx1* as a core time-conservative plant architecture

regulator. The dramatic dynamics of epistatic interactions underscore the vital role of time-dependent genetic regulation, enclosing a key gene *ZmEBF4* for early-specific plant height. Moreover, mathematical modeling quantified developmental diversity of inbred lines, enabling a predictive breeding strategy driven by ontogenic hypothesis in crop improvement.

Methods

Materials and experiment design

In the present study, a subset of 679 maize diverse inbred lines were selected randomly from the complete-diallel plus Unbalanced Breeding-derived Inter-Cross (CUBIC) population that prevalently used in genetic study of quantitative traits [19]. All inbred lines were grown in cultivated pots with 4 replicates and one plant per pot, following the complete-random experiment design. To avoid micro-environment influence among cultivated pots, two check lines- CHANG7-2 and DAN340 were randomly set among the CUBIC lines with 11 and 8 pot replications. The population pot cultivation followed the normal management.

Image analysis and i-trait extraction

All inbred lines were screened for the growth attributes using the high-throughput phenotyping (HTP) platform from seedling stage (V3) to mature stage (R3) per 3 days, totally collected phenotypic data across 18 periods. The timing of image acquisition and specific environmental information for each period are provided in Additional file

2: Table S21. The data collection was carried out from May 1, 2019, to June 27, 2019, lasting a total of 58 days. The first collection period took two days to complete with two phenotyping chambers simultaneously, while the remaining periods were completed within a single day with four phenotyping chambers simultaneously with each darkroom operating at a speed of 120 pots per hour. Each day, image acquisition started at 8:00 a.m. and ended at 5:00 p.m., lasting 9 hours. For each maize pot, 20 images were captured to ensure that the image showing the maximum projected area of the maize plant could be obtained for subsequent analysis. This scheme enabled the completion of all maize image acquisition within a single day, ensuring comparable growth trends across plants and guaranteeing high-quality images. The whole-development phenotyping collected totally 1,002,240 RGB images (~10 terabytes). The algorithm was developed based on LabVIEW (National Instruments, Inc., USA), C++, and OpenCV, and was designed for maize image segmentation and phenotypic trait extraction. The specific process included: (1) performing region segmentation on the original images to remove interfering objects such as edge tracks;(2) obtaining binary images of the whole maize plant through threshold segmentation, and calculating biomass- and structure-related traits such as plant area, height, and width;(3) calling the OpenCV dynamic link library to obtain the convex hull image and calculating a series of features related to the convex hull;(4) applying the binary image as a mask to the original image to generate RGB images containing only the target region, as well as grayscale images corresponding to the I (Intensity), H (Hue), S (Saturation), and G (Green) components, from which histogram texture

and color-related parameters are calculated. After performing image segmentation using the algorithm, some images may exhibit poor segmentation results due to noise during the image acquisition process. We manually checked all segmentation results and re-segmented the images with poor segmentation performance to ensure the quality met the expected results. To assess the segmentation performance, we randomly selected 24 images from different growth stages for evaluation. By comparing manual segmentation with algorithm-based segmentation, the Intersection over Union (IoU) was calculated to be 0.893 (Additional file 2: Table S22). The Receiver Operating Characteristic (ROC) curve evaluates the performance of the maize whole-plant segmentation model, Area Under the Curve (AUC) is 0.991, indicating excellent performance in distinguishing plant pixels (positive samples) from background/noise (negative samples) (Additional file 1: Figure S18).

Quality control for all i-trait

For each i-trait, four replicated values were collected per line. The outlier (beyond the mean value $\pm \mathbf{1.8}\boldsymbol{\sigma}$) of 4 replicated value was removed, and the mean of remaining values was treated to be i-trait phenotype. With the exception of variance component and broad-sense heritability analyses, the mean values were utilized for all subsequent analyses.

Principal component analysis

Principal component analysis was performed using the dudi.pca function from the ade4 (Version = 1.7.19) package in R language.

Definition of i-trait type

For each i-trait, the phenotypic data was normalized across inbred lines per development period. The regression slope was calculated per line based on normalized i-traits, describing the growth trend across periods. The i-trait was defined as increasing type, if more 50% of 679 lines had the slope $\geq \mathbf{0.3}$; it was decreasing type if the 50% slope were $\leq -\mathbf{0.3}$; or as stable type.

Variance component analysis

All replicate values for each line were utilized to calculate variance component of lifespan i-traits. The formula: $\boldsymbol{Y = u + G + T + G \times T + e}$. $\boldsymbol{Y}$ is the i-trait value for a genotype in a development period, $\boldsymbol{u}$ represents the grand mean, $\boldsymbol{G}$ stands for the genotype effect of the 679 lines, $\boldsymbol{T}$ denotes the temporal effect of developmental stages, $\boldsymbol{G \times T}$ is the effect from interaction between $\boldsymbol{G}$ and $\boldsymbol{T}$, $\boldsymbol{e}$ is the residual error. The model was run as fully random effects using the 'lmer' function from package 'lme4' (Version = 1.1.30) in R language.

Broad-sense heritability analysis

The formula for calculating broad-sense heritability of traits: $\boldsymbol{H^2 = \sigma_G^2 / [\sigma_G^2 + \sigma_e^2 / r]}$. $\boldsymbol{\sigma_G^2}$ and $\boldsymbol{\sigma_e^2}$ are the genotypic variance and residual variance, *r* is the number of

replications. The 'lme4' package in R language was used to evaluate the variance component.

Genome-wide association study

The whole-genome 2,822,486 SNP variants with MAF≥0.05 on the 679 maize CUBIC lines were derived from the previous study [19]. We performed genome-wide association studies (GWAS) using the univariate linear mixed model (LMM) implemented in the GEMMA software (version 0.98.1) [44] for 67 i-traits across 18 development periods. The model formula: $\boldsymbol{y} = \boldsymbol{W\alpha} + \boldsymbol{x\beta} + \boldsymbol{u} + \boldsymbol{\epsilon}$, $\boldsymbol{u} \sim \boldsymbol{MVN_n}(\mathbf{0}, \boldsymbol{\lambda\tau^{-1}K})$, $\boldsymbol{\epsilon} \sim \boldsymbol{MVN_n}(\mathbf{0}, \boldsymbol{\tau^{-1}}\mathbf{I_n})$, W is an $\boldsymbol{n} \times \boldsymbol{c}$ matrix of covariates (fixed effects) including a column of 1s. where α is a c-vector of fixed-effect coefficients, including the intercept; x denotes an n-vector of marker genotypes; β represents the effect size of the marker; u is an n-vector of random effects; ε is an n-vector of residuals; τ^{-1} is the variance of the residual errors; λ is the ratio of the two variance components; K is a known $\boldsymbol{n} \times \boldsymbol{n}$ genetic relatedness matrix; and I_n is an $\boldsymbol{n} \times \boldsymbol{n}$ identity matrix. MVN_n denotes the n-dimensional multivariate normal distribution. The random effect u was used to control the influence of population structure. The centered relatedness matrix K was computed within GEMMA using the following formula: $\boldsymbol{G_c} = \frac{\mathbf{1}}{\boldsymbol{p}}\sum_{\boldsymbol{i}=\mathbf{1}}^{\boldsymbol{p}}(\boldsymbol{x_i} - \mathbf{1}_{\boldsymbol{n}}\bar{\boldsymbol{x}}_{\boldsymbol{i}})(\boldsymbol{x_i} - \mathbf{1}_{\boldsymbol{n}}\bar{\boldsymbol{x}}_{\boldsymbol{i}})^{\boldsymbol{T}}$, we denoted $\boldsymbol{X}$ as the $\boldsymbol{n} \times \boldsymbol{p}$ matrix of genotypes, $\boldsymbol{x_i}$ as its $\boldsymbol{i}$th column representing genotypes of ith SNP, $\bar{\boldsymbol{x}}_{\boldsymbol{i}}$ as the sample mean, and $\mathbf{1}_{\boldsymbol{n}}$ as a $\boldsymbol{n} \times \mathbf{1}$ vector of 1's. The GWAS threshold for SNP significance was 3.5×10^{-7}, following the Bonferroni correction method (p=1/n,

where n is 2,822,486). Significant SNPs within a physical distance of <20 kb were initially clustered into the same locus. Subsequently, loci exhibiting significant linkage disequilibrium ($r^2 \geq 0.2$) were further merged. The resulting loci after this two-step consolidation were designated as quantitative trait loci (QTLs), with each QTL required to contain at least two significant SNPs [19] while QTLs with significant linkage disequilibrium but separated by a distance greater than 10 Mb were prohibited merged. For each i-trait, the detected original QTLs from different periods were merged into consensus QTL, if they were physical colocalization or approximation with physical distance less than 1 Mb and linkage disequilibrium ($r^2 \geq 0.2$). The most significant SNP across periods was defined to be the leading SNP for the consensus QTL. Across i-traits, the consensus QTLs with physical colocalization and sharing at least one significant SNP were further integrated into unique QTL region. The leading SNP and derived consensus QTL were selected to evaluate the genetic attributes for unique QTL. If a unique QTL was mapped by i-traits in only one development stage, it was defined as a dynamic QTL, or as a conservative QTL. If a unique QTL was mapped by at least two or more i-traits, it was defined as a pleiotropic QTL, or as a monotropic QTL. The QTL hotspot along the genome was evaluated using a 1-Mb sliding window, the intervals with top 5% QTLs counts per window was defined as the QTL hotspots. Linkage Disequilibrium (LD) between SNPs was calculated using the snpgdsLDMat function from SNPRelate (Version = 1.24.0) package.

Expression analysis

The leaves RNA-seq data of *ZmEBF4* in V9 from CUBIC panel was collected at the Hainan field station in the winter of 2016 [19]. The FPKM (Fragments Per Kilobase of transcript per Million mapped reads) of *ZmEBF4* was used as the phenotype to perform expression QTL analysis using GEMMA software [44]. The multi-tissue and multi-period expression profile data of maize B73 were obtained from the MaizeGDB website (https://maizegdb.org).

The bi-QTL Interaction analysis

For each i-trait, all QTLs that were significant at any time point in single GWAS were filtered to perform the genetic interaction analysis between the leading SNPs of these QTLs (referred to as bi-QTLs) for all development periods. A two-way ANOVA was used to test the bi-SNP interaction using the 'anova' function in R language, as following formula: $\boldsymbol{Y = G_1 + G_2 + G_1 \times G_2 + e}$. $\boldsymbol{Y}$ is the phenotypic value for each genotype in all time point, $\boldsymbol{G_1}$ is the main genetic effect of the first SNP, $\boldsymbol{G_2}$ the main genetic effect of another SNP, $\boldsymbol{G_1 \times G_2}$ is the interaction effect between two SNPs, $\boldsymbol{e}$ is the residual error. To control the false positive rate, we applied a multiple testing correction to the significance threshold. Specifically, we first scanned the number of bi-QTL pairs tested for each trait and selected the maximum value (435) to perform a uniform Bonferroni correction. The adjusted significance threshold was set at $\boldsymbol{\alpha = 0.05/435}$. Bi-QTLs with a p-value exceeding this threshold were defined as statistically significant epistatic interactions. Due to the time-specific nature of the QTLs—where a locus may be significant only at certain developmental stages—we

categorized bi-QTL interactions into three types based on the individual significance of each constituent QTL at the time of testing: interactions between two significant QTLs (SS), interactions between one significant and one non-significant QTL (SN), interactions between two non-significant QTLs (NN).

Gene function verification of *ZmEBF4*

The EMS mutant *ebf4* (Mutant ID: EMS4-1a0572) with a G to A mutation at 346 aa, resulting in an early stop codon, was obtained from a maize EMS mutant library (https://elabcaas.cn/memd/public/index.html#/) [45], which was sequenced to confirm the mutation. The KASP (kompetitive allele specific PCR) Primers was designed for genotyping of segregated offsprings. Purified progeny was obtained from backcrossing homozygous mutant with wild type twice in Hainan and Xiangyang province, China. The field phenotype of mutant, WT and mutant/WT was identified in Xiangyang, Jilin and Hainan, which occurred in July 2023, August 2024 and December 2024 respectively.

Gene function verification of *ZmGalOx1*

Using the Jing724 inbred line as the target material, we employed CRISPR–CasY7, a gene-editing system independently developed by WIMI Biotechnology Co., Ltd. to generate a precise editing event in *ZmGalOx1*, resulting in a frameshift mutant designated as *ZmGalOx1*-KO^{Jing724}. A total of 20 pots each of the *ZmGalOx1*-KO^{Jing724} and wild-type Jing724 were cultivated in an outdoor greenhouse under management

practices consistent with those used in the 2019 experiment. From May 19 to July 28, 2025, image-based phenotyping was performed at seven-day intervals using the same image acquisition and analysis protocols as those applied in 2019.

Growth trajectory and parameter analysis

In order to find the i-trait possessing growth pattern, a typical growth model Gompertz [46] ($\boldsymbol{y = A_{max} e^{-be^{-rt}}}$) was used, which was a modified S-curve. Here, $\boldsymbol{y}$ is the phenotypic value of i-trait in time point $\boldsymbol{t}$ ($\boldsymbol{t^{th}}$ day after sowing), the model has three parameters: $\boldsymbol{A_{max}}$ (the phenotypic value in the moment when growth stop); $\boldsymbol{b}$ (determining the position of the curve along the time axis); $\boldsymbol{r}$ (the growth rate in fastest growing moment). For each i-trait from 18 time point, the growth curves of all genotypes were fitted, and $\boldsymbol{R^2}$ was used to evaluate the fitting effect of each growth curve. Then based on the mean value of fitting $\boldsymbol{R^2}$ from all inbred line, the i-trait was filtered to be a trait possessing growth pattern if $\boldsymbol{R^2}$ was bigger than 0.9. For further extraction of growth features, a principal component analysis (PCA) was used to acquire the key features from all i-trait reflecting growth. The first two principal components PC1 and PC2 were selected to fit final growth trajectory of all genotypes. Based on the distribution of all inbred lines (Fig. 6a), the quadratic function model ($\boldsymbol{y = ax^2 + bx + c}$) was used to fit the growth trajectory. Here, $\boldsymbol{y}$ is the value of PC2, $\boldsymbol{x}$ is the value of PC1, the model has three parameters: $\boldsymbol{a}$ (determining the direction and size of opening), $\boldsymbol{b}$ (determining the tangent slope at the intersection of the model and the y-axis), $\boldsymbol{c}$ (determining the intersection of the model and the

y-axis). And the model has two feature parameters: $-\frac{b}{2a}$ (determining the position of the axis of symmetry), $c-\frac{b^2}{4a}$ (determining the location of extreme value). The optimal parameter values were estimated using function from stats (Version = 4.0.0) package in R with Nelder-Mead method [47]. Colocalized QTL identification between growth parameters and i-trait was consistent with the unique QTL identification.

Growth trajectory complement analysis of hybrids

The genomic prediction of the hybrids' trajectory parameters was performed using the mixed.solve function from rrBLUP (Version = 4.6.1) package. The genetic relatedness of parental lines from each hybrids was computed within GEMMA using the following formula: $\boldsymbol{G_c = \frac{1}{p}\sum_{i=1}^{p}\frac{1}{v_{x_i}}(x_i - 1_n\bar{x}_i)(x_i - 1_n\bar{x}_i)^T}$, we denoted $\boldsymbol{X}$ as the $\boldsymbol{n \times p}$ matrix of genotypes, $\boldsymbol{x_i}$ as its $\boldsymbol{i}$th column representing genotypes of ith SNP, $\bar{\boldsymbol{x}}_{\boldsymbol{i}}$ as the sample mean and $\boldsymbol{v_{x_i}}$ as the sample variance of $\boldsymbol{i}$th SNP, and $\mathbf{1}_{\boldsymbol{n}}$ as a $\boldsymbol{n \times 1}$ vector of 1's.

Hypothesis testing and multiple comparisons

The test method of significance is Wilcoxon-Mann-Whitney with two-tailed approach from geom_signif function of R package ggsignif (Version = 0.6.3). The method of multiple comparisons is Least Significant Difference from LSD.test function of R package agricolae (Version = 1.3.5).

Acknowledgements

We would like to thank Mr. Hao Liu from the National Key Laboratory of Crop Genetic Improvement for essential help in running the high-throughput computing clusters.

Authors' contributions

Yingjie Xiao, Wanneng Yang and Jianbing Yan designed and supervised this study. Chengxiu Wu performed most of genetic statistical analysis work, Zedong Geng is primarily responsible for all image analysis and trait extraction work. Weikun Li, Junli Ye, Tianjin Xie, Xiaoyuan Hao, Yunyu Chen, Yuanyuan Chen participated in the early-stage material cultivation and image detection work. Yuanhao Du, Cheng Ma, Yu Gao, Yuyue Chen and Yupeng Liu participated in the functional verification work of *ebf4* gene. Songtao Gui, Jingyun Luo participated in the genetic statistical analysis work. Wenyu Yang contributed to the analysis of growth trajectories. Jieting Xu, Minliang Jin and Xiaoyu Wu provided the genetic materials to validate the function of *ZmGalOx1*. Chengxiu Wu prepared the manuscript. All authors critically read, revised and approved the manuscript.

Funding

This work was supported by the National Natural Science Foundation of China (32321005, 32472136, U21A20205), the National Key Research and Development Program of China (2022YFD1201502), the Key Agricultural Core Technology Research Project in Hubei Province (HBNYHXGG2023-9), Fundamental Research Funds for the Central Universities (2662024ZKPY003).

Availability of data and materials

The selected images showing the maximum projected area of individual maize plants have been uploaded to Zenodo platform [48]. The image analysis and i-trait extraction pipeline and codes followed the previous procedure [18] without any modifications and has been publicly released at Github [49] and Zenodo [50] platform, all code in the repository are released under the MIT License. Genotypic and RNA-seq data from CUBIC panel were available from Dataset NCBI [51] in a previous study [19]. Agronomic phenotype from CUBIC panel were downloaded from Additional file 4 in a previous study [19, 52]. Genotypic and phenotypic data for 6,210 hybrids and their parental lines are available from Dataset ZEAMAP [53] in a previous study [20].

Declarations

Supplementary Information

Additional file 1: Figure S1-18. All supplementary figures cited in main text.

Additional file 2: Table S1-22. All supplementary tables cited in main text.

Additional file 3: Video. Demo of high-throughput image acquisition process.

Ethics approval and consent to participate

Not applicable.

Consent for publication

Not applicable.

Competing interests

The authors from all affiliations declare that they have no competing interests.

Author details

[1]National Key Laboratory of Crop Genetic Improvement, Huazhong Agricultural University, Wuhan, 430070, China. [2]Hubei Hongshan Laboratory, Wuhan 430070, China. [3]Wuhan Agri-matrix Technology Co., Ltd., 430070, China. [4]Shandong Agricultural University, Taian 271018, China. [5]Guangdong Academy of Agricultural Sciences, Guangzhou 510640, China. [6]WIMI Biotechnology Co., Ltd., Qingdao, Shandong, 266000, China.

Peer review information

Wenjing She was the primary editor of this article and managed its editorial process and peer review in collaboration with the rest of the editorial team. The peer-review history is available in the online version of this article.

References

1. Hickey LT, N. Hafeez A, Robinson H, Jackson SA, Leal-Bertioli SCM, Tester M, Gao C, Godwin ID, Hayes BJ, Wulff BBH: **Breeding crops to feed 10 billion.** *Nature Biotechnology* 2019, **37:**744-754. https://doi.org/10.1038/s41587-019-0152-9
2. Ray DK, Ramankutty N, Mueller ND, West PC, Foley JA: **Recent patterns of crop yield growth and stagnation.** *Nature Communications* 2012, **3**.

https://doi.org/10.1038/ncomms2296
3. Liang Y, Liu HJ, Yan J, Tian F: **Natural Variation in Crops: Realized Understanding, Continuing Promise.** *Annu Rev Plant Biol* 2021, **72:**357-385. https://doi.org/10.1146/annurev-arplant-080720-090632
4. Liu J, Fernie AR, Yan J: **The Past, Present, and Future of Maize Improvement: Domestication, Genomics, and Functional Genomic Routes toward Crop Enhancement.** *Plant Commun* 2020, **1:**100010. https://doi.org/10.1016/j.xplc.2019.100010
5. Boyle EA, Li YI, Pritchard JK: **An Expanded View of Complex Traits: From Polygenic to Omnigenic.** *Cell* 2017, **169:**1177-1186. https://doi.org/10.1016/j.cell.2017.05.038
6. Xiao Y, Tong H, Yang X, Xu S, Pan Q, Qiao F, Raihan MS, Luo Y, Liu H, Zhang X, et al: **Genome-wide dissection of the maize ear genetic architecture using multiple populations.** *New Phytol* 2016, **210:**1095-1106. https://doi.org/10.1111/nph.13814
7. Liu X, Li YI, Pritchard JK: **Trans Effects on Gene Expression Can Drive Omnigenic Inheritance.** *Cell* 2019, **177:**1022-1034 e1026. https://doi.org/10.1016/j.cell.2019.04.014
8. Yang W, Feng H, Zhang X, Zhang J, Doonan JH, Batchelor WD, Xiong L, Yan J: **Crop Phenomics and High-Throughput Phenotyping: Past Decades, Current Challenges, and Future Perspectives.** *Mol Plant* 2020, **13:**187-214. https://doi.org/10.1016/j.molp.2020.01.008
9. Bac-Molenaar JA, Vreugdenhil D, Granier C, Keurentjes JJ: **Genome-wide association mapping of growth dynamics detects time-specific and general quantitative trait loci.** *J Exp Bot* 2015, **66:**5567-5580. https://doi.org/10.1093/jxb/erv176
10. Neumann K, Klukas C, Friedel S, Rischbeck P, Chen D, Entzian A, Stein N, Graner A, Kilian B: **Dissecting spatiotemporal biomass accumulation in barley under different water regimes using high-throughput image analysis.** *Plant Cell Environ* 2015, **38:**1980-1996. https://doi.org/10.1111/pce.12516
11. Wang X, Wang H, Long Y, Liu L, Zhao Y, Tian J, Zhao W, Li B, Chen L, Chao H, Li M: **Dynamic and comparative QTL analysis for plant height in different developmental stages of Brassica napus L.** *Theor Appl Genet* 2015, **128:**1175-1192. https://doi.org/10.1007/s00122-015-2498-9
12. Pauli D, Andrade-Sanchez P, Carmo-Silva AE, Gazave E, French AN, Heun J, Hunsaker DJ, Lipka AE, Setter TL, Strand RJ, et al: **Field-Based High-Throughput Plant Phenotyping Reveals the Temporal Patterns of Quantitative Trait Loci Associated with Stress-Responsive Traits in Cotton.** *G3 (Bethesda)* 2016, **6:**865-879. https://doi.org/10.1534/g3.115.023515
13. Neumann K, Zhao Y, Chu J, Keilwagen J, Reif JC, Kilian B, Graner A: **Genetic architecture and temporal patterns of biomass accumulation in spring barley revealed by image analysis.** *BMC Plant Biol* 2017, **17:**137.

https://doi.org/10.1186/s12870-017-1085-4

14. Camargo AV, Mackay I, Mott R, Han J, Doonan JH, Askew K, Corke F, Williams K, Bentley AR: **Functional Mapping of Quantitative Trait Loci (QTLs) Associated With Plant Performance in a Wheat MAGIC Mapping Population.** *Front Plant Sci* 2018, **9:**887. https://doi.org/10.3389/fpls.2018.00887
15. Ren T, Hu Y, Tang Y, Li C, Yan B, Ren Z, Tan F, Tang Z, Fu S, Li Z: **Utilization of a Wheat55K SNP Array for Mapping of Major QTL for Temporal Expression of the Tiller Number.** *Front Plant Sci* 2018, **9:**333. https://doi.org/10.3389/fpls.2018.00333
16. Adak A, Murray SC, Washburn J: **Deciphering temporal growth patterns in maize: integrative modeling of phenotype dynamics and underlying genomic variations.** *New Phytologist* 2024. https://doi.org/10.1111/nph.19575
17. Anderson SL, 2nd, Murray SC, Chen Y, Malambo L, Chang A, Popescu S, Cope D, Jung J: **Unoccupied aerial system enabled functional modeling of maize height reveals dynamic expression of loci.** *Plant Direct* 2020, **4:**e00223. https://doi.org/10.1002/pld3.223
18. Wu X, Feng H, Wu D, Yan S, Zhang P, Wang W, Zhang J, Ye J, Dai G, Fan Y, et al: **Using high-throughput multiple optical phenotyping to decipher the genetic architecture of maize drought tolerance.** *Genome Biol* 2021, **22:**185. https://doi.org/10.1186/s13059-021-02377-0
19. Liu HJ, Wang X, Xiao Y, Luo J, Qiao F, Yang W, Zhang R, Meng Y, Sun J, Yan S, et al: **CUBIC: an atlas of genetic architecture promises directed maize improvement.** *Genome Biol* 2020, **21:**20. https://doi.org/10.1186/s13059-020-1930-x
20. Xiao Y, Jiang S, Cheng Q, Wang X, Yan J, Zhang R, Qiao F, Ma C, Luo J, Li W, et al: **The genetic mechanism of heterosis utilization in maize improvement.** *Genome Biol* 2021, **22:**148. https://doi.org/10.1186/s13059-021-02370-7
21. Yang W, Guo T, Luo J, Zhang R, Zhao J, Warburton ML, Xiao Y, Yan J: **Target-oriented prioritization: targeted selection strategy by integrating organismal and molecular traits through predictive analytics in breeding.** *Genome Biol* 2022, **23:**80. https://doi.org/10.1186/s13059-022-02650-w
22. Zhang X, Huang C, Wu D, Qiao F, Li W, Duan L, Wang K, Xiao Y, Chen G, Liu Q, et al: **High-Throughput Phenotyping and QTL Mapping Reveals the Genetic Architecture of Maize Plant Growth.** *Plant Physiol* 2017, **173:**1554-1564. https://doi.org/10.1104/pp.16.01516
23. Guo Z, Yang W, Chang Y, Ma X, Tu H, Xiong F, Jiang N, Feng H, Huang C, Yang P, et al: **Genome-Wide Association Studies of Image Traits Reveal Genetic Architecture of Drought Resistance in Rice.** *Mol Plant* 2018, **11:**789-805. https://doi.org/10.1016/j.molp.2018.03.018
24. Yang W, Guo Z, Huang C, Duan L, Chen G, Jiang N, Fang W, Feng H, Xie W, Lian X, et al: **Combining high-throughput phenotyping and genome-wide association studies to reveal natural genetic variation in rice.** *Nat Commun*

2014, **5:**5087. https://doi.org/10.1038/ncomms6087

25. Muszynski MG, Dam T, Li B, Shirbroun DM, Hou Z, Bruggemann E, Archibald R, Ananiev EV, Danilevskaya ON: **delayed flowering1 Encodes a basic leucine zipper protein that mediates floral inductive signals at the shoot apex in maize.** *Plant Physiol* 2006, **142:**1523-1536. https://doi.org/10.1104/pp.106.088815
26. Moose SP, Sisco PH: **Glossy15, an APETALA2-like gene from maize that regulates leaf epidermal cell identity.** *Genes & Development* 1996, **10:**3018-3027. https://doi.org/10.1101/gad.10.23.3018
27. Liang Y, Liu Q, Wang X, Huang C, Xu G, Hey S, Lin HY, Li C, Xu D, Wu L, et al: **ZmMADS69 functions as a flowering activator through the ZmRap2.7-ZCN8 regulatory module and contributes to maize flowering time adaptation.** *New Phytol* 2019, **221:**2335-2347. https://doi.org/10.1111/nph.15512
28. Tian J, Wang C, Chen F, Qin W, Yang H, Zhao S, Xia J, Du X, Zhu Y, Wu L, et al: **Maize smart-canopy architecture enhances yield at high densities.** *Nature* 2024. https://doi.org/10.1038/s41586-024-07669-6
29. Yan Y, Duan F, Li X, Zhao R, Hou P, Zhao M, Li S, Wang Y, Dai T, Zhou W: **Photosynthetic capacity and assimilate transport of the lower canopy influence maize yield under high planting density.** *Plant Physiology* 2024, **195:**2652-2667. https://doi.org/10.1093/plphys/kiae204
30. Makarevitch I, Thompson A, Muehlbauer GJ, Springer NM: **Brd1 gene in maize encodes a brassinosteroid C-6 oxidase.** *PLoS One* 2012, **7:**e30798. https://doi.org/10.1371/journal.pone.0030798
31. Soyk S, Lemmon ZH, Sedlazeck FJ, Jimenez-Gomez JM, Alonge M, Hutton SF, Van Eck J, Schatz MC, Lippman ZB: **Duplication of a domestication locus neutralized a cryptic variant that caused a breeding barrier in tomato.** *Nat Plants* 2019, **5:**471-479. https://doi.org/10.1038/s41477-019-0422-z
32. Wei X, Chen M, Zhang Q, Gong J, Liu J, Yong K, Wang Q, Fan J, Chen S, Hua H, et al: **Genomic investigation of 18,421 lines reveals the genetic architecture of rice.** *Science* 2024, **385:**eadm8762. https://doi.org/10.1126/science.adm8762
33. Li W, Ma M, Feng Y, Li H, Wang Y, Ma Y, Li M, An F, Guo H: **EIN2-directed translational regulation of ethylene signaling in Arabidopsis.** *Cell* 2015, **163:**670-683. https://doi.org/10.1016/j.cell.2015.09.037
34. Gagne JM, Smalle J, Gingerich DJ, Walker JM, Yoo SD, Yanagisawa S, Vierstra RD: **Arabidopsis EIN3-binding F-box 1 and 2 form ubiquitin-protein ligases that repress ethylene action and promote growth by directing EIN3 degradation.** *Proc Natl Acad Sci U S A* 2004, **101:**6803-6808. https://doi.org/10.1073/pnas.0401698101
35. Binder BM, Walker JM, Gagne JM, Emborg TJ, Hemmann G, Bleecker AB, Vierstra RD: **The Arabidopsis EIN3 binding F-Box proteins EBF1 and EBF2 have distinct but overlapping roles in ethylene signaling.** *Plant Cell*

2007, **19:**509-523. https://doi.org/10.1105/tpc.106.048140

36. Geng Z, Lu Y, Duan L, Chen H, Wang Z, Zhang J, Liu Z, Wang X, Zhai R, Ouyang Y, Yang W: **High-throughput phenotyping and deep learning to analyze dynamic panicle growth and dissect the genetic architecture of yield formation.** *Crop and Environment* 2024, **3:**1-11. https://doi.org/10.1016/j.crope.2023.10.005
37. Yu X, Yin D, Nie C, Ming B, Xu H, Liu Y, Bai Y, Shao M, Cheng M, Liu Y, et al: **Maize tassel area dynamic monitoring based on near-ground and UAV RGB images by U-Net model.** *Computers and Electronics in Agriculture* 2022, **203**. https://doi.org/10.1016/j.compag.2022.107477
38. Quan L, Feng H, Lv Y, Wang Q, Zhang C, Liu J, Yuan Z: **Maize seedling detection under different growth stages and complex field environments based on an improved Faster R–CNN.** *Biosystems Engineering* 2019, **184:**1-23. https://doi.org/10.1016/j.biosystemseng.2019.05.002
39. Xiao Y, Liu H, Wu L, Warburton M, Yan J: **Genome-wide Association Studies in Maize: Praise and Stargaze.** *Mol Plant* 2017, **10:**359-374. https://doi.org/10.1016/j.molp.2016.12.008
40. McMullen MD, Kresovich S, Villeda HS, Bradbury P, Li H, Sun Q, Flint-Garcia S, Thornsberry J, Acharya C, Bottoms C, et al: **Genetic properties of the maize nested association mapping population.** *Science* 2009, **325:**737-740. https://doi.org/10.1126/science.1174320
41. Dell'Acqua M, Gatti DM, Pea G, Cattonaro F, Coppens F, Magris G, Hlaing AL, Aung HH, Nelissen H, Baute J, et al: **Genetic properties of the MAGIC maize population: a new platform for high definition QTL mapping in Zea mays.** *Genome Biol* 2015, **16:**167. https://doi.org/10.1186/s13059-015-0716-z
42. Kover PX, Valdar W, Trakalo J, Scarcelli N, Ehrenreich IM, Purugganan MD, Durrant C, Mott R: **A Multiparent Advanced Generation Inter-Cross to fine-map quantitative traits in Arabidopsis thaliana.** *PLoS Genet* 2009, **5:**e1000551. https://doi.org/10.1371/journal.pgen.1000551
43. Chen R, Deng Y, Ding Y, Guo J, Qiu J, Wang B, Wang C, Xie Y, Zhang Z, Chen J, et al: **Rice functional genomics: decades' efforts and roads ahead.** *Sci China Life Sci* 2022, **65:**33-92. https://doi.org/10.1007/s11427-021-2024-0
44. Zhou X, Stephens M: **Genome-wide efficient mixed-model analysis for association studies.** *Nat Genet* 2012, **44:**821-824. https://doi.org/10.1038/ng.2310
45. Lu X, Liu J, Ren W, Yang Q, Chai Z, Chen R, Wang L, Zhao J, Lang Z, Wang H, et al: **Gene-Indexed Mutations in Maize.** *Mol Plant* 2018, **11:**496-504. https://doi.org/10.1016/j.molp.2017.11.013
46. Gompertz B: **XXIV. On the nature of the function expressive of the law of human mortality, and on a new mode of determining the value of life contingencies. In a letter to Francis Baily, Esq. F. R. S. &c.** *Philosophical Transactions of the Royal Society of London* 1997, **115:**513-583. https://doi.org/10.1098/rstl.1825.0026

47. Nelder JA, Mead R: **A Simplex Method for Function Minimization.** *The Computer Journal* 1965, **7:**308-313. https://doi.org/10.1093/comjnl/7.4.308
48. Wu C, Geng Z, Li W, Ye J, Hao X, Xu J, et al. Genetic dynamics drive maize growth and breeding. Datasets. Zenodo. https://zenodo.org/records/18150504. (2026.01.05).
49. Wu C, Geng Z, Li W, Ye J, Hao X, Xu J, et al. Genetic dynamics drive maize growth and breeding. Github. https://github.com/gengzedong/Genetic-dynamics-drive-maize-growth-and-breeding. (2026.01.05).
50. Wu C, Geng Z, Li W, Ye J, Hao X, Xu J, et al. Genetic dynamics drive maize growth and breeding. Zenodo. https://zenodo.org/records/18151471. (2026.01.05).
51. Liu H-J, Wang X, Xiao Y, Luo J, Qiao F, Yang W, Zhang R: CUBIC: an atlas of genetic architecture promises directed maize improvement. Dataset NCBI: https://www.ncbi.nlm.nih.gov/bioproject/PRJNA597703 (2020a).
52. Liu H-J, Wang X, Xiao Y, Luo J, Qiao F, Yang W, Zhang R: CUBIC: an atlas of genetic architecture promises directed maize improvement. https://static-content.springer.com/esm/art%3A10.1186%2Fs13059-020-1930-x/MediaObjects/13059_2020_1930_MOESM4_ESM.xlsx (2020a).
53. Xiao Y, Jiang S, Cheng Q, Wang X. The genetic mechanism of heterosis utilization in maize improvement. Genotypic and phenotypic data for inbred lines and hybrids. Dataset ZEAMAP. 2021b. http://zeamap.hzau.edu.cn/ftp/99_MaizegoResources/01_CUBIC_related/. Accessed 25 Apr 2021.

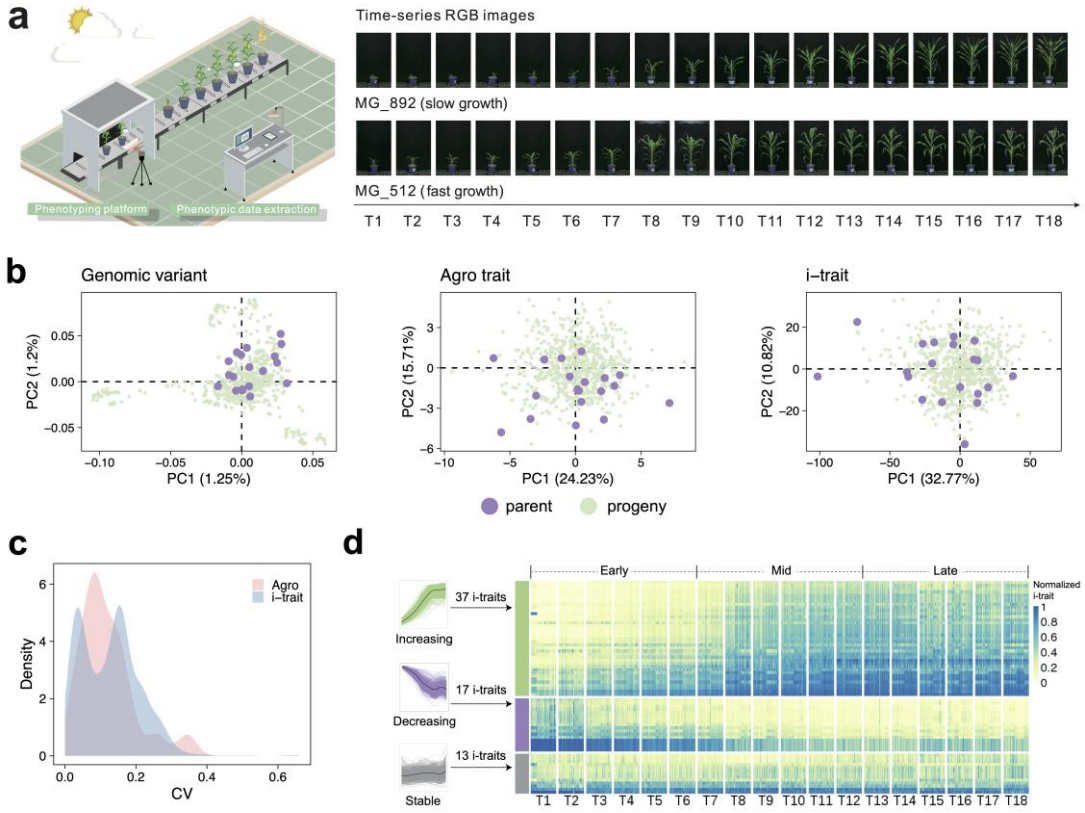

Fig. 1. Diverse and dynamic variation of i-traits across maize inbred lines during whole-growth periods. a, The workflow of the image-based traits collected by the high-throughput phenotyping platform. Two inbred lines with slow and fast growth, MG_892 and MG_512, were exhibited based on the RGB images of the plant along the 18-time points. **b**, The PCA analysis of 679 inbred lines based on the genomic variants, agronomic traits and i-traits, respectively. The 20 parents and 659 progeny lines were indicated with different colors. **c**, The comparison of coefficient of variation between agronomic traits and i-traits. **d**, The three typical growth modes for inbred lines via continuous i-trait data. The heatmap plot indicated the normalized i-trait value from 679 inbred lines in 18 time points.

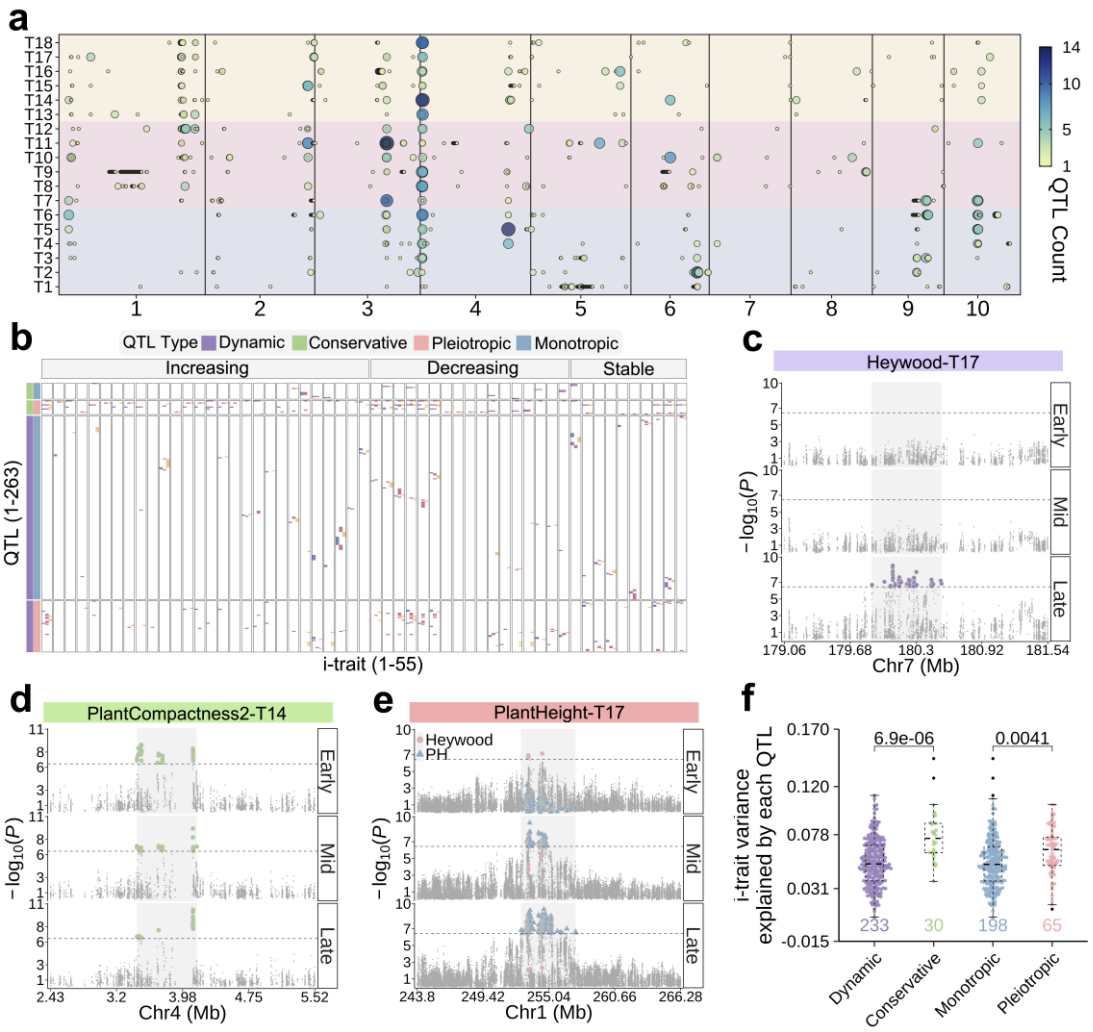

Fig. 2. The genetic dynamics of maize i-trait variations cross development periods. a, Genome-wide QTL summary for all i-traits across 18 growth periods. At each period, the size and color of bubble indicates the count of QTLs in a sliding window of 1Mb across the genome. **b**, The overview of four types of QTLs reflecting the i-trait dynamics. All QTLs detected in 55 i-traits across 18 periods were merged into 263 unique QTLs. For one i-trait, a QTL was defined to be the dynamic QTL if only detected in one growth period, or as conservative QTL. On the other hand, one QTL can be defined as the pleiotropic QTL if detected in multiple i-traits either within or cross periods, or as the monotropic QTL. Colored cells represent significantly association, with colors indicating different developmental stages: blue for Early, red

for Mid, and yellow for Late. **c-e**, Regional Manhattan plots for three key QTLs responsible for the genetic dynamics. In alphabetical order, the panel indicated the dynamic, conservative and cross-period pleiotropic QTL, the colored dots indicated the values above the GWAS threshold, the shaded area denoted the QTL interval. **f**, The difference of i-trait variances explained by four types of QTLs. The Wilcoxon-Mann-Whitney with two-tailed method was used to evaluate the significance of differences between dynamic and conservative QTLs, as well as between pleiotropic and monotropic QTLs.

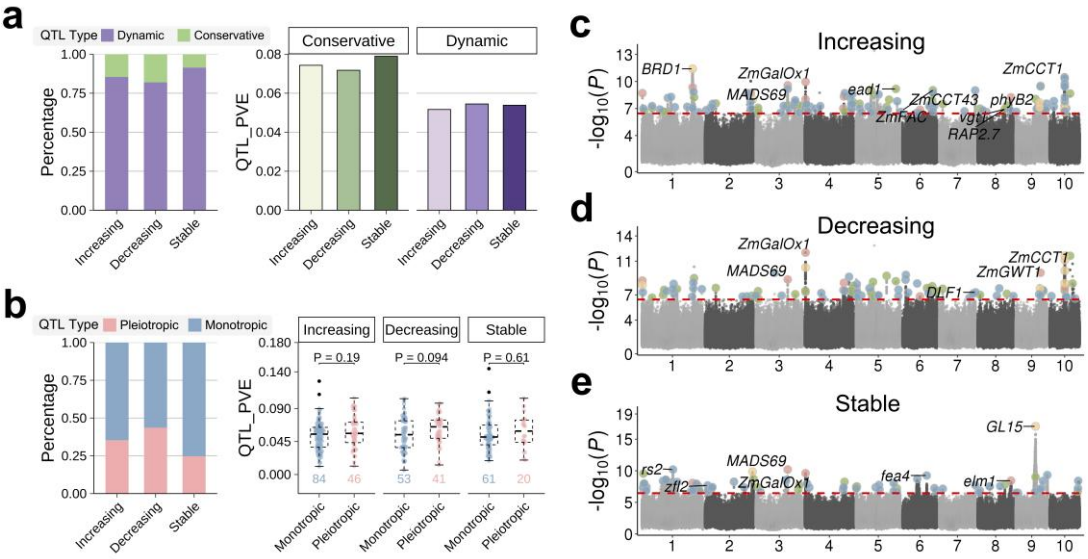

Fig. 3. The distinctive genetics of three i-trait growth types in maize. a, The preference of QTL dynamics by three growth types of i-traits. **b**, The preference of QTL pleiotropy by three growth types of i-traits. **c-e**, Integrated GWAS results of all i-traits from three growth types. The dashed horizontal line indicated the GWAS threshold (p=3.5×10^{-7}), the most significant SNP of each i-trait was indicated as the colored dot, while the colors represented the four QTL types (blue – dynamic and

monotropic, green – dynamic and pleiotropic, yellow – conservative and monotropic, red – conservative and pleiotropic).

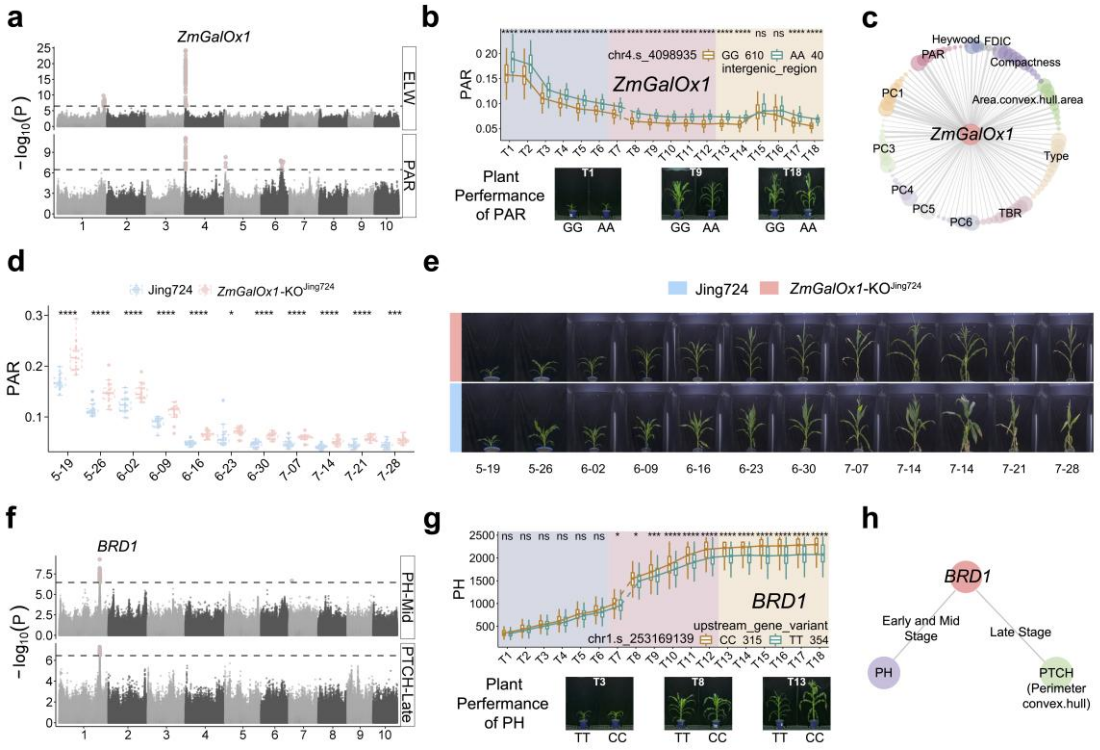

Fig. 4. Rediscovering novel function of *ZmGalOx1* and *BRD1* via i-traits across periods. a, GWAS colocalization of ear leaf width and PAR in late phase. **b**, The haplotypic effects of *ZmGalOx1* on PAR trait across 18 time points. **c**, The functional network of *ZmGalOx1* on multiple i-traits across periods. The node colors indicated different i-traits, the node size indicated the different periods. **d**, Comparison of PAR i-trait among *ZmGalOx1*-KO^{Jing724} and Jing724 across 11 time points from May 19 to July 28, 2025 at Wuhan from China, '*' denotes p<=0.05, '**' denotes p<=0.01, '***' denotes p<=0.001, '****' denotes p<=0.0001. The test method of significance is Student's t-test with two-tailed approach. **e**, Comparison of RGB images among *ZmGalOx1*-KO^{Jing724} and Jing724 across 11 time points from May 19 to July 28, 2025

at Wuhan from China. **f**, GWAS colocalization of plant height in the middle phase and PTCH in late phase. **g**, The haplotypic effects of *BRD1* on plant height across 18 time points. **h**, Functional relocation of *BRD1* on multiple traits across periods. PH denotes plant height, ELW denotes ear leaf width, PAR denotes the perimeter/projected area ratio, PTCH denotes the perimeter_convex.hull.

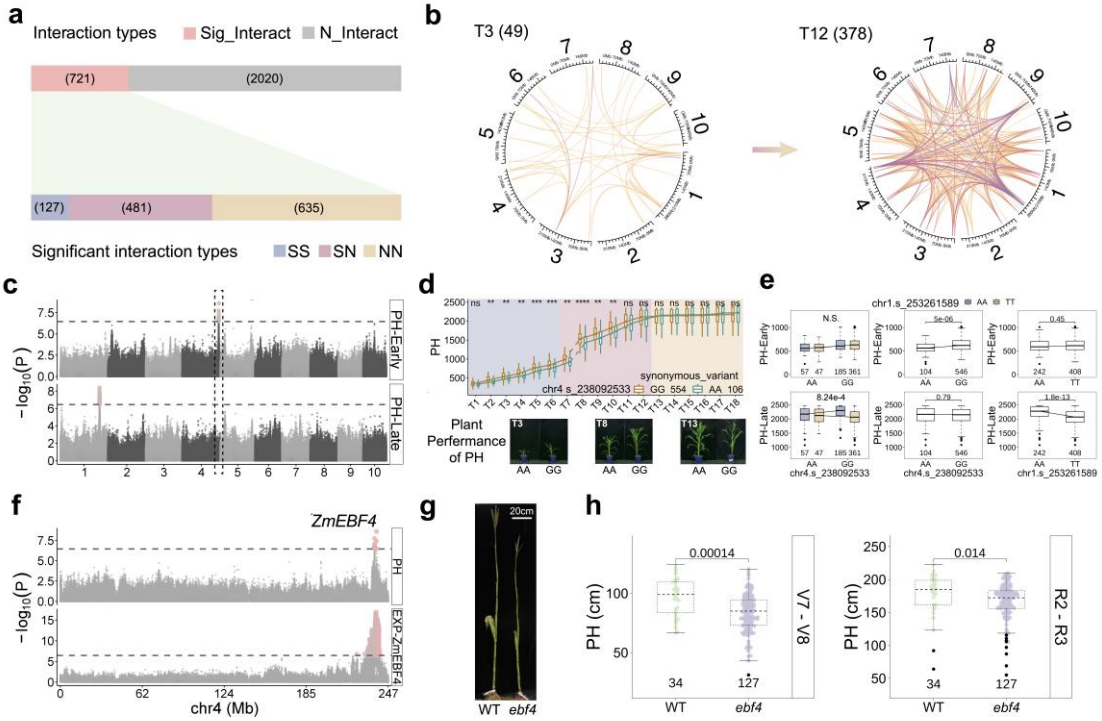

Fig. 5. Cross-period remodeling interactions explained the early-specific effect of *ZmEBF4* on plant height in maize. a, Interaction types between QTLs (bi-QTLs) detected across the whole periods, bi-QTLs exceeding the significance threshold (p<=1.15e-4) were defined as Sig_Interact, which were categorized into three types based on the individual significance of each constituent QTL: SS (both QTLs significant), SN (only one QTL significant) and NN (neither QTL significant). **b**, The variation of genome-wide interactions between early and late stages. The colored line

indicated the interaction type, and the line width indicated the significance of the interaction. **c**, GWAS colocalization of PH in early and late phase. **d**, The haplotypic effects of chr4.s_238092533 on plant height across 18 time points. **e**, The haplotype effects of chr4.s_238092533 and chr1.s_253261589 on plant height, along with their epistatic interaction effects in early and late stages, the genotypes of line B73 is GG (chr4.s_238092533) and TT (chr1.s_253261589). **f**, GWAS colocalization of PH and expression level of *ZmEBF4*, colored dot represents the SNP above the threshold. **g**, Field-grown picture of WT and mutant line of *ZmEBF4* in Hainan, scale bar corresponds to 20cm. **h**, Comparison of PH among mutant line of *ZmEBF4* and WT on V7-V8 and R2-R3 at Hainan from China. PH denotes plant height.

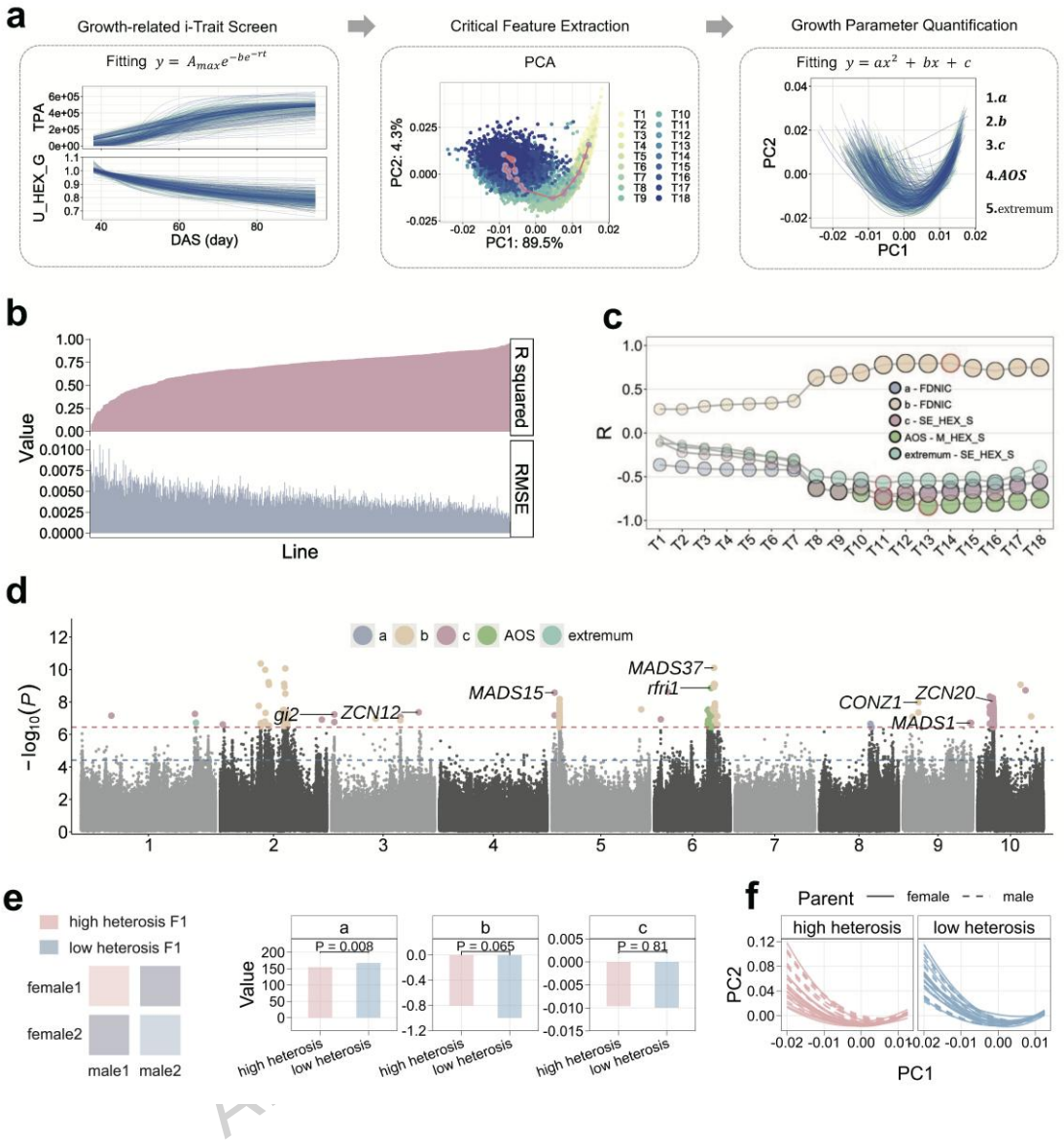

Fig. 6. The trajectory modeling integrating growth variation empower the breeding design. a, Schematic diagram of growth trajectory modeling and parameter quantification. **b**, Model fitting performance of growth trajectories across all inbred lines. **c**, The identification of the i-trait and period most correlated with growth parameters. The size and color density of the dots indicated the absolute value of the correlation coefficient. The dot with red border indicated the highest correlated period. **d**, GWAS results of five trajectory parameters. The significant SNPs were indicated with colored dots that grouped by different parameters. The red dashed horizontal line

indicated the GWAS threshold ($p \leq 3.5 \times 10^{-7}$), suggestive threshold ($p \leq 3.9 \times 10^{-5}$) was denoted as blue dashed horizontal line. AOS denotes axis of symmetry. **e**, The comparison of predicted trajectory parameters between the hybrids with high and low heterosis. **f**, The potential of hybrid design via trajectory complements between female and male parents.